Supplementary File

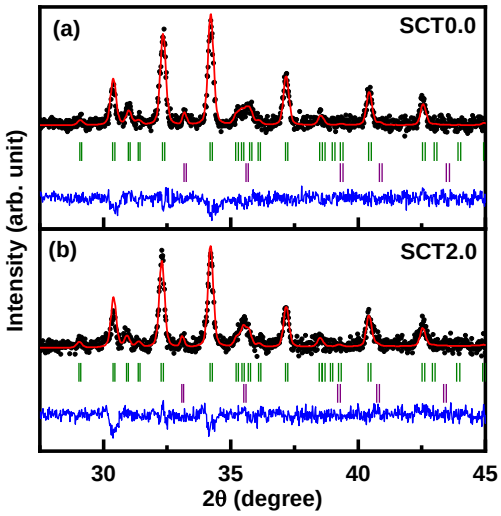


Figure S1. Rietveld refinement of the XRD pattern of (a) SCT0.0 and (b) SCT2.0. Both the systems contain hexagonal M-type ferrite phase with $P6_3/mmc$ space group symmetry (shown in green Braggs' positions) and α-Fe_2O_3 phase with R-3c space group symmetry (shown in purple Braggs' positions).

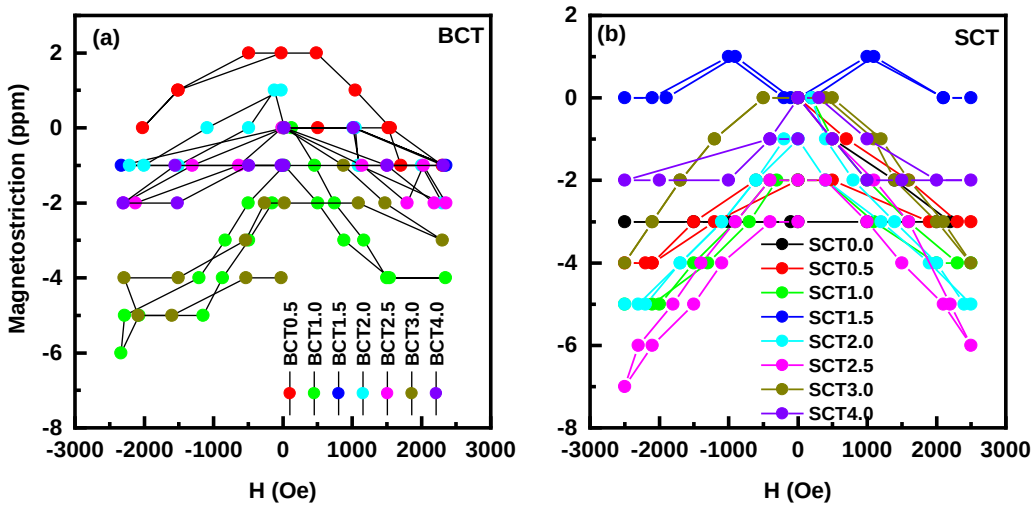


Figure S2. Magnetic field dependence of the magnetostriction of (a) BCTx and (b) SCTx samples.

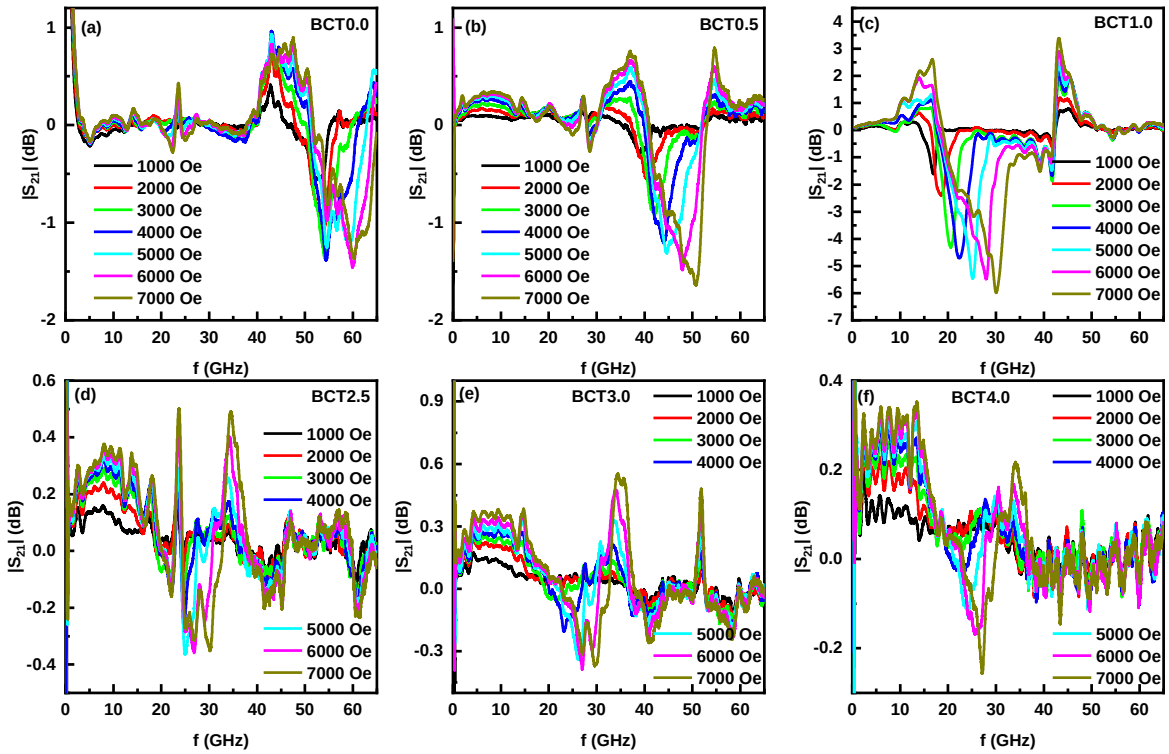


Figure S3. S_{21} vs. f profiles of different BCTx samples at selected magnetic fields.

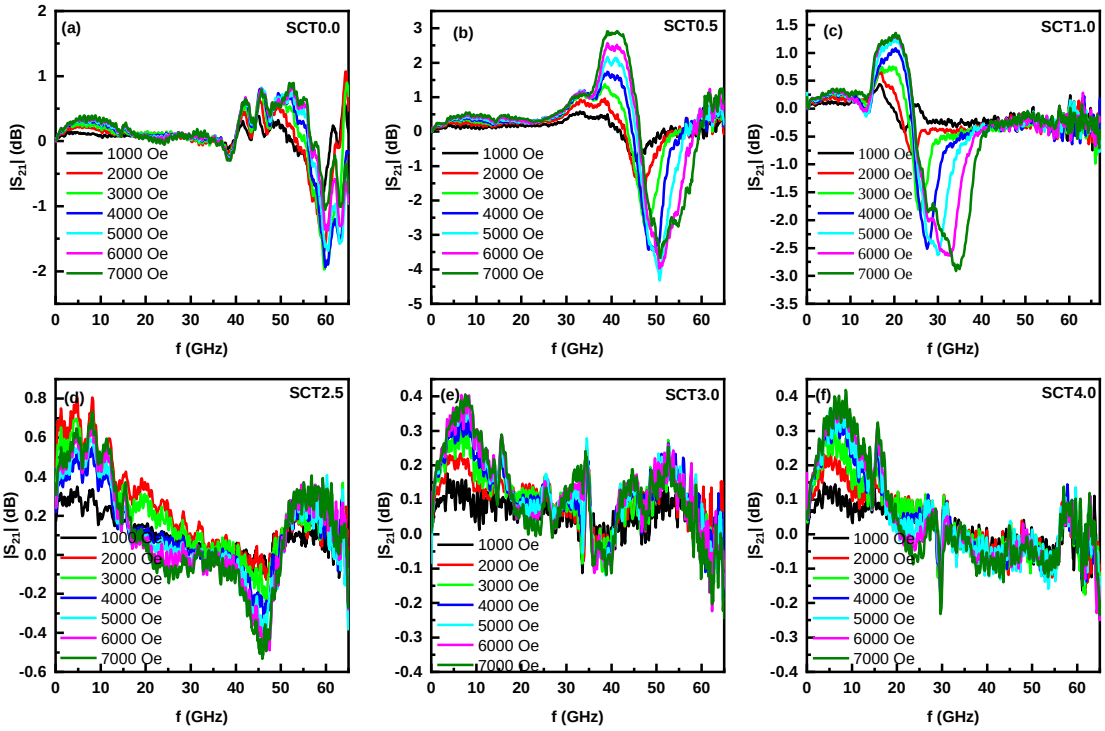


Figure S4. S21 vs. f profiles of different SCTx samples at selected magnetic fields.

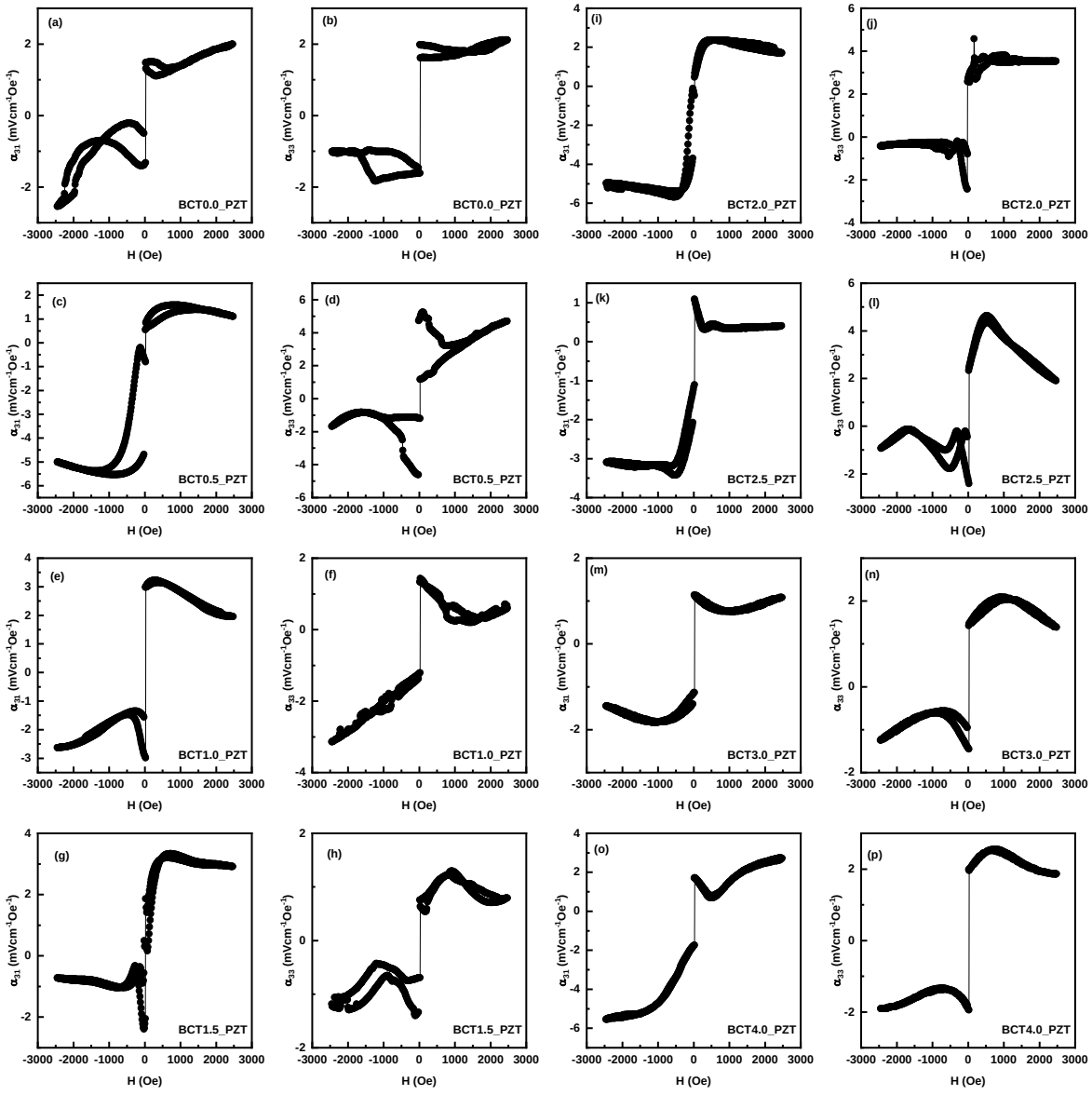


Figure S5. MEVC for BCTx-PZT bilayers for in-plane and out of plane magnetic fields.

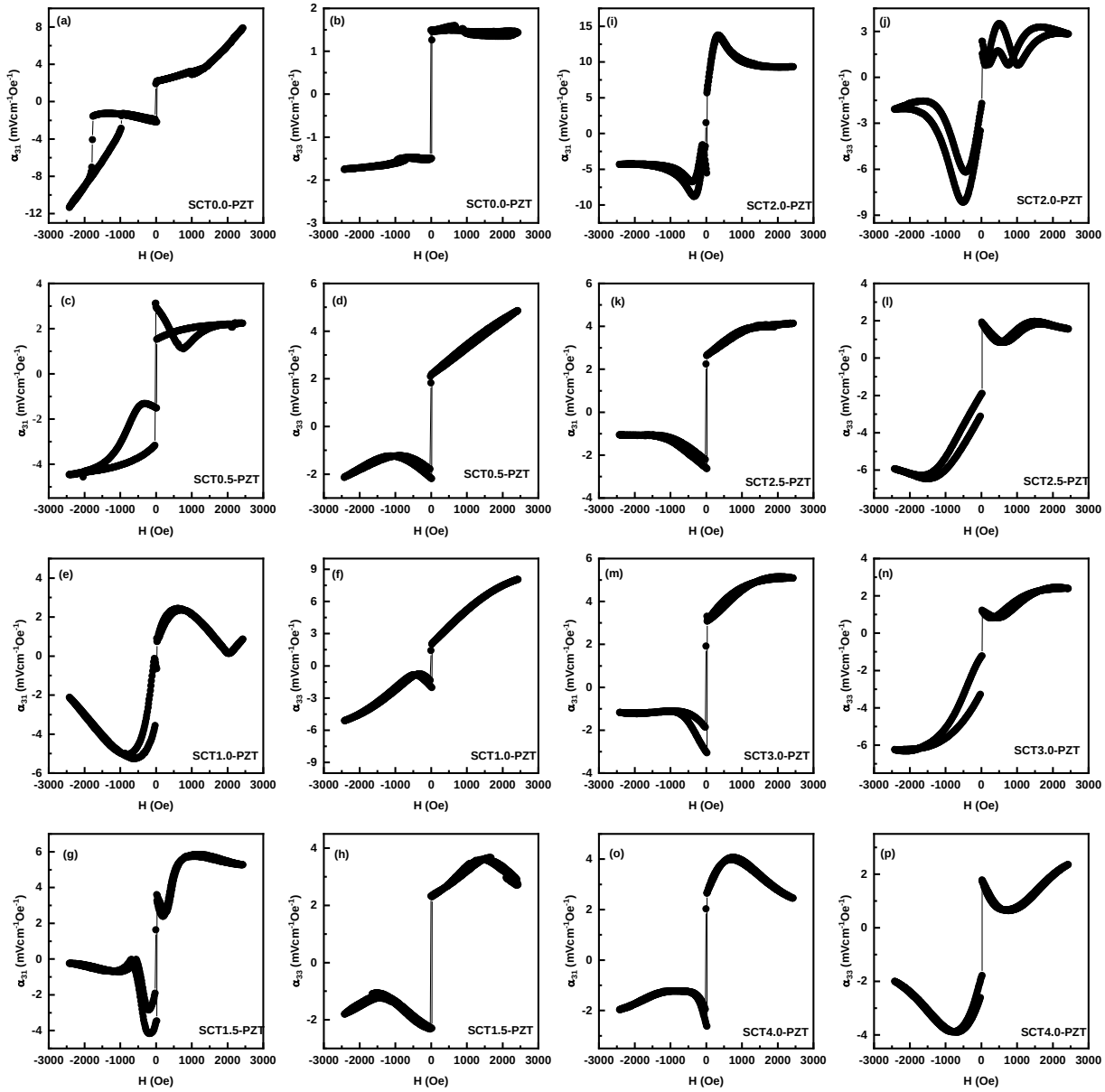


Figure S6. MEVC for SCTx-PZT bilayers for in-plane and out of plane magnetic fields.

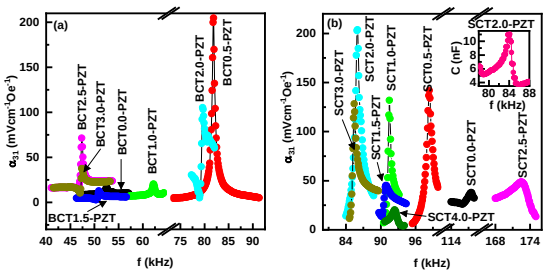


Figure S7. MEVC plots of (a) BCTx-PZT and (b) SCTx-PZT bilayer composite samples as a function of frequency near EMR. In the inset of (b) the variation of the capacitance of PZT layer attached to the SCT2.0-PZT bilayer is shown.

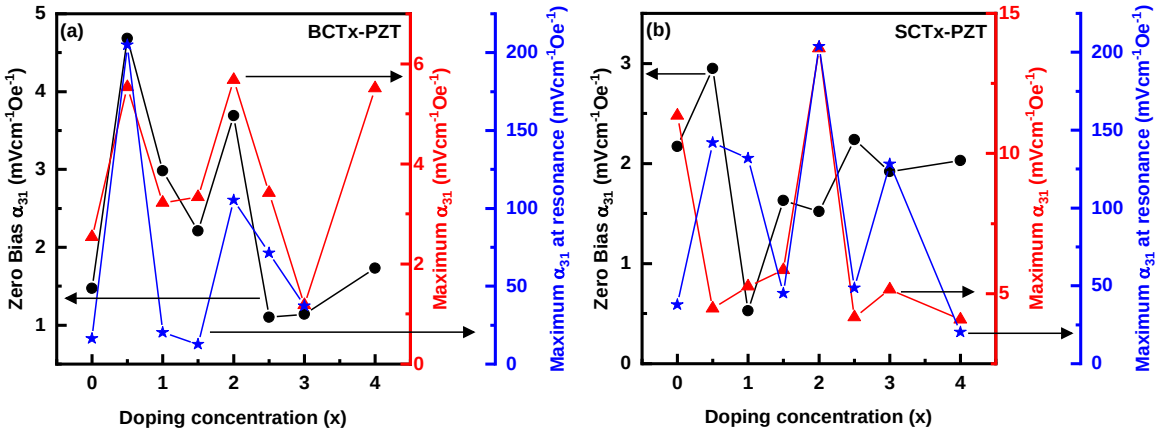


Figure S8. Zero-bias MEVC, MEVC at EMR and maximum achievable MEVC in field scan for SCTx-PZT bilayer composites.